ARCHIVIO ISTITUZIONALE
DELLA RICERCA

Alma Mater Studiorum Università di Bologna
Archivio istituzionale della ricerca

Performance and total warming impact assessment of pure fluids and mixtures replacing HFCs in micro-ORC energy systems

This is the final peer-reviewed author's accepted manuscript (postprint) of the following publication:

Published Version:
Bianchi, M., Branchini, L., De Pascale, A., Melino, F., Ottaviano, S., Peretto, A., et al. (2022). Performance and total warming impact assessment of pure fluids and mixtures replacing HFCs in micro-ORC energy systems. APPLIED THERMAL ENGINEERING, 203, 1-13 [10.1016/j.applthermaleng.2021.117888].

Availability:
This version is available at: https://hdl.handle.net/11585/877561 since: 2024-05-14

Published:
DOI: http://doi.org/10.1016/j.applthermaleng.2021.117888

Terms of use:

Some rights reserved. The terms and conditions for the reuse of this version of the manuscript are specified in the publishing policy. For all terms of use and more information see the publisher's website.

This item was downloaded from IRIS Università di Bologna (https://cris.unibo.it/).
When citing, please refer to the published version.

(Article begins on next page)

17 September 2026

Performance and total warming impact assessment of pure fluids and mixtures replacing HFCs in micro-ORC energy systems

Michele Bianchi, *Lisa* Branchini, *Andrea* De Pascale, *Francesco* Melino, *Saverio* Ottaviano, *Antonio* Peretto and *Noemi* Torricelli

Università di Bologna – DIN, Viale del Risorgimento 2, 40136 Bologna, Italia

Abstract. The use of the micro-ORC (Organic Rankine Cycle) technology for waste-heat recovery and distributed generation is generally considered a viable and promising low-carbon solution, in the framework of combined heat and power and renewable energy applications. However, micro-ORCs environmental impact, due to high-GWP (global warming potential) working fluid leak rates, is an issue still to overcome. At the same time, numerical studies reveal that low-GWP fluids do not always guarantee the same performance of typically used fluids, leading to additional use of conventional fuels in combustion-based energy systems, to compensate the lower power production. This study proposes a comprehensive evaluation of the actual greenhouse effect related to the operation of ORC systems in the kW scale. The method is derived from the TEWI (total equivalent warming impact) concept for refrigeration systems, since it includes both direct and indirect contributions to the greenhouse gas emission related to the ORC system. A comparison between traditional HFC-134a (R134a) and some of its low-GWP replacements has been performed, accounting for the effect of the operating fluid leakage during system operation, but also for the indirect contribution associated to the lower performance that can be achieved using more sustainable working fluids, such as hydrofluoroolefins (HFO). Alternative fluids that have been tested are two pure compounds (R1234yf and R1234ze(E)), and four mixtures (R134a-R1234yf; R-134a-R1234ze(E); R515A; R430A). A semi-empirical lumped-parameters model has been employed for simulating the behavior of the ORC system. For the model validation, the experimental data collected on a reference 2-kW ORC test bench with R-134a have been used. The model was then applied to investigate the performance of the system working with alternative fluids. The results show that the indirect emissions associated to HFOs may lead to higher values of total equivalent CO_2 emissions, with respect to the employment of R134a as working fluid. The main factors affecting the environmental evaluation, such as emission factors, fluid leak rate and R134a concentration in the mixture, can be decisive and are discussed in this work.

Keywords: micro-ORC, low-GWP fluids, HFO, R134a mixtures, semi-empirical model, total equivalent warming impact

Introduction

Climate change is acknowledged as a tangible issue that must be addressed to avoid major environmental consequences in the next future. Recent policy decisions set the reduction of greenhouse gas (GHG) emissions as key strategic target for 2030 [1]. Experts agree that main potential solutions to achieve this goal rely on: the improvement in the systems conversion efficiency, the increase of renewables in the energy mix and the on-site generation of electricity [1]. Waste-heat recovery and in particular power generation from low-grade heat sources (with temperature level below 200 °C) is gaining interest as a viable mean to implement the aforementioned solutions. In this context, the Organic Rankine Cycle (ORC) technology is one of the most suitable energy conversion option for valorising low-grade heat and producing electricity or useful mechanical power. The savings potential associated with micro-to-small scale ORC is believed to be enormous [2].

The working fluid selection represents a key decision for an ORC arrangement, affecting the system design and the related performance [2]. In particular, synthetic refrigerants belonging to hydrofluorocarbons (HFCs) category, such as R245fa, R123 and R134a [3] appear to be very performing for low-temperature applications thanks to their low critical temperature. On the other hand, previous state-of-the-art HFCs, despite their null

ozone depletion potential, risk to highly contributing to the anthropogenic greenhouse effect, if released, due to their high values of global warming potential (GWP) and high residence time in the atmosphere [4]. For this reason, at the beginning of the XXI century, the European Union started taking measures to phase out the use of these GHGs. The current phase-down regime [5] is a step-by-step approach with the objective of reducing the average GWP of the refrigerants available in the market, through the allocation of quotas by the European Commission to producers and importers of bulk HFCs. The initiative provides for a decrease of the consumption of common HFCs of 79% by 2030. This means that industry, and refrigerant users in general, are forced to undergo a transition toward new and low-GWP fluids. Expected average GWP of refrigerants, according to the "F-gas" regulation, and the relative equivalent carbon emissions are shown in Fig. 1 (data are elaborated from [5]).

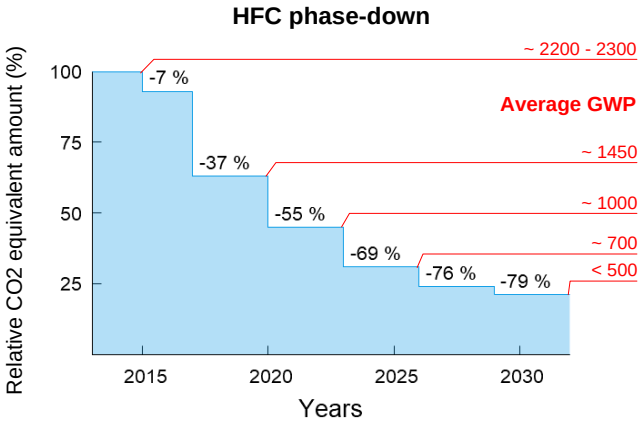

Fig. 1. Steps of HFCs phase-down, elaborated according to EU "F-gas" regulation [5].

Thus, refrigeration industry is currently working on finding valuable alternatives to HFCs, which can guarantee the same performance but lower environmental impact at the same time. In particular, potential substitutes of HFCs have been identified in the hydrofluoroolefins (HFOs) [6]. While refrigeration plants retrofit with HFOs has been already comprehensively assessed in many studies (see for example the experimental studies by Zilio et al. [7], for air conditioning, by Lee and Jung [8], for car conditioning, by Navarro-Esbrì et al. [9] and [10], on R134a replacement in compressors), dedicated and extensive tests for ORC applications are still required. Only some early studies, carried out in specific limited conditions, revealed that low-GWP fluids could not guarantee the same performance of HFC fluids. For example Invernizzi et Al. [11] investigated the potential replacement of HFC-134a (or R134a) in an ORC geothermal plant fed with hot water at 150 °C, by new HFOs, observing a decrease in the net power production. Likewise, Boyaghchi et Al. [12] performed a multi-objective optimization of a novel micro combined cooling, heating and power system supplied by solar and geothermal energy, with four working fluids including R134a, R423A, R1234ze(E) and R1234yf. Their results indicate that the best fluid from the energy and exergy viewpoints is R134a. Other studies have been conducted on the topic, but mainly based on a pure thermodynamic approach, adopting simplified hypotheses such as constant expander and pump efficiency and adiabatic expansion process [13], [14], [15]. Indeed, it is crucial to properly include into the assessment the actual influence of the fluid on performance of the key ORC components. Actual operating conditions of expander and pump can strongly depend on fluid properties such as density and viscosity, especially if considering volumetric type machines, as demonstrated in previous work of the Authors [16]. When considering the expander real operating conditions, another important factor of influence is the fluid thermal conductivity, as the expansion process cannot be considered adiabatic [17]. To perform a fair comparison between high and low-GWP refrigerants as ORC working fluids, a rigorous environmental investigation should be included in the analysis. Indeed, in some cases, the single assessment based on GWP value may not consider indirect effects, such as the loss of performance of the system using more sustainable fluids, which can be associated to an additional contribution of indirect emissions, unless the energy gap is fulfilled by means of fully renewable sources.

In view of the above, the aim of this study is to propose a comprehensive evaluation of the actual greenhouse impact of micro-ORC systems, when operated with low-GWP working fluids in low-temperature heat recovery applications. The method is derived from the TEWI (total equivalent warming impact) concept for refrigeration systems, since it includes both direct and indirect contributions to the greenhouse gas emission related to the

ORC system. Direct emissions are associated to the leakage of refrigerant during the system operation. The indirect contribution accounts for the emissions related to the resulting lack of power production, caused by the adoption of a less performing fluid. In the Authors knowledge, the open literature lacks studies of working fluid selection that takes into account a comprehensive greenhouse impact assessment.

Pure fluids and also binary mixtures are both taken into account for sake of completeness in this study. Use of mixtures in ORC for waste-heat-recovery applications have been proposed by several studies, especially with the aim to exploit zeotropic mixtures thermodynamic properties, capable to optimize the heat transfer process at the evaporator and condenser of the ORC, see for example the study by Andreasen et al. [18] on binary mixtures of hydrocarbons. Fluid blends of different refrigerants are considered in this GHG analysis, since it cannot be excluded a priori that optimal or mid-term sub-optimal solutions to limit total carbon emissions could consist in blending current low-GWP fluids with the high performing HFC fluids. In addition, in Authors opinion, literature still lacks in studies investigating especially the potential of specific mixtures of R134a blended with HFOs, or other potential R134a substitutive mixtures.

This analysis, in particular, takes as a reference a typical architecture of micro-ORC system, presented in [19], for which reliable experimental data related to the use of R134a as working fluid are already available. Indeed, the reference system is designed to work with R134a but also with fluids with similar properties, such as the HFOs R1234yf and R1234ze(E), according to the manufacturer [20]. The first step consists in assessing the micro-ORC performance when working with low-GWP substitutes of R134a (both pure fluids and mixtures) in a realistic application. A semi-empirical model of the whole system has been implemented and validated with experimental data, collected operating with the conventional fluid R134a. Semi-empirical model type is chosen as this demonstrated to be the most suitable modelling approach for similar applications, with robust prediction in both fitting and extrapolation more than usually adopted constant efficiency models [21]. Indeed, this kind of models allows to account for actual operating conditions of the volumetric machines and not only for the only thermodynamic process. Adaptations necessary to model low-GWP fluids and blends instead of R134a have been also discussed and introduced to the aforementioned model. The last step comprises the simulation of the plant behaviour over a typical annual operation, in order to determine the yearly energy production and related GHG emissions. More in detail, the examined operating conditions refer to an existing micro-ORC operation, installed at a pool centre [22]. The system is conceived to exploit a geothermal liquid-dominated well hot source, while the cold sink is the swimming pool heating circuit.

1 Reference micro-ORC system

The reference system is a kW-scale recuperated ORC (see Fig. 2), conceived for low-grade heat sources, with temperature below 100 °C. The key component of the system is the expander, a reciprocating piston model with three cylinders placed radially at 120°, with total displacement equal to 230 cm^3 (see patent [20]).The admission and the discharge of the vapour in the expander are executed by rotary valves, which are placed in correspondence of the cylinder head and are driven by the crankshaft rotation. The expander is directly coupled with the generator, which is connected to an electrical load made of five pure resistive loads, connected in parallel between them and in delta with the generator output three-phase line. In this configuration, the load does not allow setting the generator rotational speed nor the load torque, and the expander shaft is free to achieve the equilibrium between the generator torque and the set load resistance. The other main components of the system are: the evaporator, a brazed plate heat exchanger (model Onda S202 with 64 plates); the feed pump, an external gear pump with displacement of 80 cm^3; the recuperator, a brazed plate heat exchanger (Onda S202 with 19 plates); the water condenser, a shell-and-tube heat exchanger (model Onda CT292-1100) and a liquid receiver with volume of 19 liters. The ORC pump is driven by an asynchronous electric motor, to which the pump shaft is coupled through a speed reducer with gear ratio of 1:3. The pump motor is driven by a frequency inverter, which allows the regulation of the flow rate of the working fluid. The thermal input to the ORC circuit is provided by a pressurized water heated by an electric heater with power up to 42 kW. The cooling system consists in cold water extracted from a well.

The test bench is fully equipped with an acquisition system, made of T-type thermocouples (immersion probes), ceramic pressure transducers and a Coriolis mass flow meter. Voltage and current transducers are installed on expander and pump supply lines for acquiring electrical power and frequency of the two machines. On hot and cold water circuits, K-type thermocouples (immersion probes) and magnetic flow meters are installed.

In order to collect data in specific testing conditions, the following main parameters can be controlled from the outside: the water temperature at the evaporator inlet, T_{H2Ohot}, the water flow rate at the evaporator inlet,

$\dot{m}_{H2Ohot}$, the water temperature at the condenser inlet, $T_{H2Ocold,}$ the water flow rate at the condenser inlet, $\dot{m}_{H2Ocold,}$ the feed pump frequency, f_{pp}, and the number of activated loads, n_{loads}. A full characterization of the reference ORC test bench working with R134a in steady state conditions is presented in [19].

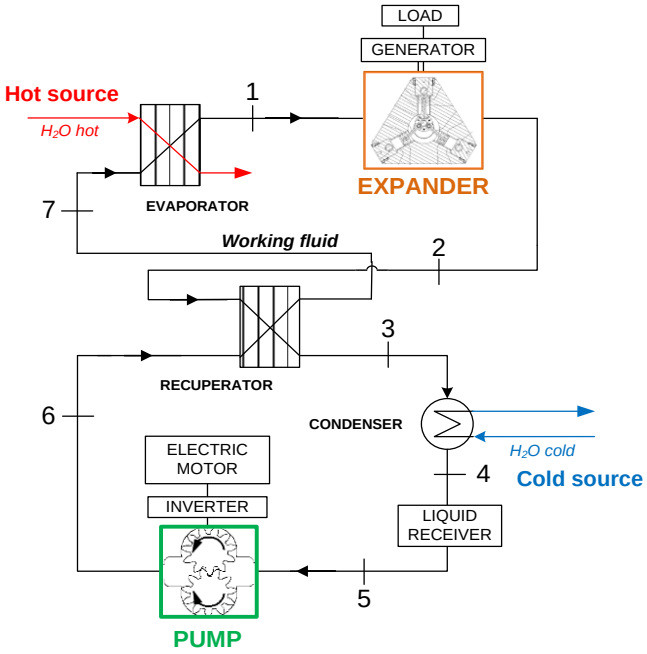

Fig. 2. Micro-ORC system simplified layout.

2 Methodology

2.1 Micro-ORC performance model

A schematic of the system model, describing the components sub-models and relationships between them, is shown in Fig. 3. Five sub-models compose the ORC model and are connected to each other: the pump and the circuit resistance ("PP & RES"), the expander ("EXP"), the recuperator ("REC"), the evaporator ("EV") and the condenser ("CD") sub-model (see the workflow in Fig. 3). The model is based on a lumped parameters approach and it allows to calculate the complete thermodynamic state of the ORC system using, as input, the boundary conditions only, i.e. the heat source and the heat sink supply conditions (T_{H2Ohot}, $\dot{m}_{H2Ohot}$, $T_{H2Ocold}$ and $\dot{m}_{H2Ocold}$), the feed pump frequency (f_{pp}) and the expander load resistance (n_{loads}). An additional input is the subcooling degree of the working fluid at the condenser outlet, ΔT_{sc}. The latter could be otherwise calculated as function of fluid charge and cold source temperature [23]. The outputs of the model are the fluid thermodynamic states in all the main sections of the cycle and, in particular, indicators, namely, the thermal input provided at the evaporator, $\dot{Q}_{ev}$, the condenser discharged heat, $\dot{Q}_{cd}$, the electric power output, $\dot{W}_{exp}$, and the pump absorbed power, $\dot{W}_{pp}$.

Since the ORC model is formulated as an implicit problem, its solution is determined through an iterative process, whose iterative variables are the condensing pressure, p_{cd}, and the expander inlet temperature, T_1. More in detail, the iterative cycle on the expander inlet temperature is nested into the condensing pressure iterative cycle. A first attempt solution of T_1 and p_{cd} is chosen by the code to start the resolution algorithm, respecting the physical constraints of the problem. As first step, the code solves the models of the pump, and runs the nested iterative cycle including the expander and the recuperator models. Output of the iterative cycles are the updated value of T_1 and p_{cd}; these values are compared with their attempt solution to evaluate whether the residual satisfy the convergence criterion or not until convergence is reached. As long as the cycles run, the attempt solutions are replaced at each iteration with their updated value.

A semi-empirical approach is chosen for each component. This kind of models rely on a set of physically meaningful equations whose parameters can be tuned to fit a reference dataset (or imposed, where known). In this study, experimental data on the reference test rig, collected during experiments carried out with R134a [19], have been considered for the calibration. The list of empirical parameters with their calibrated values are

provided in Tab. 1 for each sub-model (see "Nomenclature" and next paragraphs for detailed parameters naming and meaning). It must be highlighted that some of the empirical parameters are only size-dependent (as for example the pump cubic capacity, V_{cc}), and can be considered independent from the working fluid, while other parameters are associated to the working fluid thermodynamic characteristics. Thus, specific fluid-corrections/scaling equations are introduced for these parameters, to account for the use of fluids different from R134a, for which the model was calibrated originally. A more detailed description of each sub-model, its parameters and their correction is reported in the following sub-paragraphs.

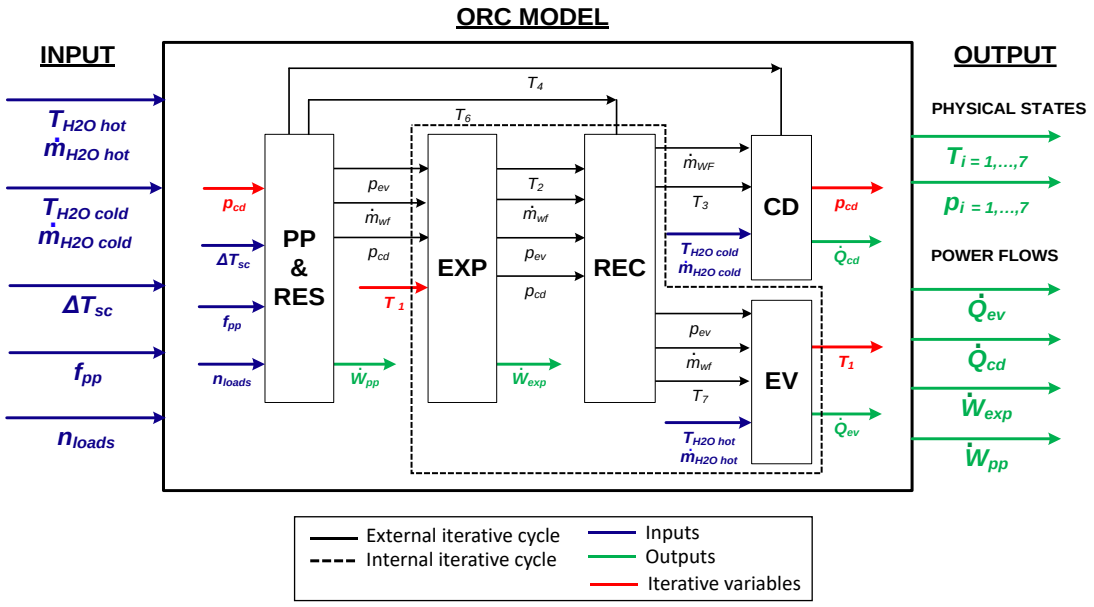

Fig. 3. The micro-ORC model schematic diagram (input are indicated in blue, iterative variables in red, intermediate variables in black and output of the model in green).

Tab. 1. Model parameters for each micro-ORC system component.

Component	Parameter	Value	Unit
Expander (EXP) [27]	A_{su}	1.47e-05	m^2
	A_{leak}	5.51e-06	m^2
	$AU_{su,ref}$	5.65e-05	W/K
	$AU_{ex,ref}$	9.23e-05	W/K
	AU_{amb}	0.96	W/K
	$r_{v,exp}$	1.459	-
	$r_{v,comp}$	1.25	-
	V_0	2.32e-08	m^3
	$W_{loss,ref}$	0.198	W
	$W_{loss,N}$	1.07e-05	W/min
Heat exchangers (EV, CD, REC)	$\alpha_{wf,ref}$	15.72, for EV/CD 4.79, for REC	$kW/m^2/K$
	$\dot{m}_{wf,ref}$	0.123	kg/s
	z	0.74	-
	$\Delta T_{sat,ref}$	20	°C
	y	-0.84	-
Pump & Circuit resistance (PP & RES)	c_1	5.29e+02	(-)
	c_2	5.10 e+02	(m^{-3})
	V_{cc}	62.3	(cm^3)
	c_3	1.52	$(m^{-1}\cdot s^{-1})$
	c_4	53.3	$(m^{-1}\cdot s^{-1})$

2.1.1 Heat exchangers

In their normal operation, ORC evaporator and condenser are interested by phase-change. The approach used to calculate the performance of evaporator and condenser is based on a three-zone lumped-parameters moving boundary model with variable heat transfer coefficients, and it is schematized in Fig. 4. According to this method, the heat exchangers are split into three different heat transfer regions (named as: SC – Subcooling zone, TP - Two Phase zone and SH – Superheating zone, in Fig. 4); the boundaries of the zones are defined by the thermodynamic phase change points of the working fluid.

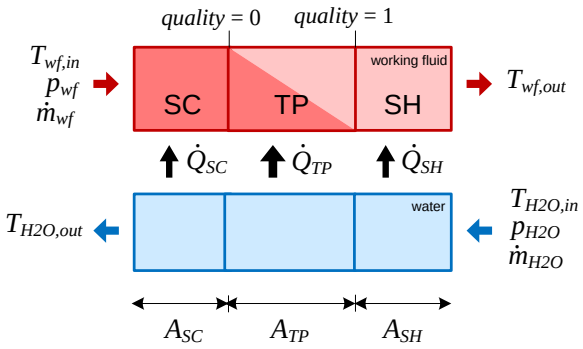

Fig. 4. Heat exchangers moving boundary model scheme.

Each zone is characterized by a global heat transfer coefficient U_i and by a heat transfer surface area A_i. According to the moving boundary approach, spatial position of each zone and its heat transfer surface (A_i) are not known a priori, but they are determined along the calculation based on the fluid state. A boundary condition is required to calculate the area of each section. The constraint is that the sum of the single surface areas corresponds to the geometrical surface area of the component, A, which is instead a model parameter.

The heat transfer occurring in the *i-th* zone is given by the product between the global heat transfer coefficient, the surface area and the logarithmic mean temperature difference $\Delta T_{log,i}$ of the zone (Eq. (1)).

$$\dot{Q}_i = A_i U_i \cdot \Delta T_{log,i} \tag{1}$$

The considered global heat transfer coefficient accounts for the convective coefficient of the working fluid side, α_{wf}, and the convective coefficient of the water side, α_{H2O} (Eq. (2)). Conductive heat transfer contribution have been considered negligible, due to high value of steel conductive coefficient and thin wall thickness.

$$U_i = \left(\frac{1}{\alpha_{wf,i}} + \frac{1}{\alpha_{H2O,i}} \right)^{-1} \tag{2}$$

The water convective coefficients, and the working fluid convective coefficients for subcooling and superheating zone, are determined by means of the Dittus-Boelter correlation for forced convection [24]. The working fluid convective coefficient for the two-phase zone, $\alpha_{wf,TP}$, derives instead from empirical correlations. In particular, correlation used for the evaporator has the form of Eq. (3).

$$\alpha_{wf,TP} = \alpha_{wf,TP,ref} \left(\frac{\dot{m}_{wf}}{\dot{m}_{wf,ref}} \right)^{z} \left(\frac{\Delta T_{sat}}{\Delta T_{sat,ref}} \right)^{y} \tag{3}$$

where $\alpha_{wf,ref}$ represents the value of the convective coefficient in reference operating conditions. In off-design conditions, $\alpha_{wf,ref}$ is adjusted according to the so called “thermal resistance scaling” method, to account for the dependence of the convective coefficient from the fluid velocity [26]. Following this method, the reference point convective heat transfer coefficients, $\alpha_{wf,ref}$, is scaled as function of the ratio between the actual mass flow rate, $\dot{m}_{wf}$, and the one calculated in the reference point, $\dot{m}_{wf,ref}$, raised to power z. This

exponent usually does not differ too much from 0.8, which corresponds to the exponent for the Reynolds number in the Dittus Boelter correlation. According to empirical observations, an additional correction term accounting for the nucleated boiling phenomenon is introduced to better estimate the variation of the evaporator heat transfer coefficient when the operating conditions differ from the reference one. Assuming a forced convection boiling regime, the nucleated boiling convection weight is proportional to the difference between the working fluid saturation temperature and the secondary fluid temperature, ΔT_{sat} [24]. Thus, the term $\left(\frac{\Delta T_{sat}}{\Delta T_{sat,ref}}\right)^{y}$ in eq. 3 accounts for the modification of ΔT_{sat} with respect to its reference value $\Delta T_{sat,ref}$ and its influence on the nucleated boiling heat transfer contribution. Both z and y values are obtained by interpolating the available experimental data (the resulting values are reported in Tab. 1).

Correlation used for the condenser is the same of Eq. (3), but in this case pure convective regime is assumed, thus, excluding the dependence from ΔT_{sat}. As a result, condenser two-phase working fluid convective coefficient is estimated by means of Eq. (4).

$$\alpha_{wf} = \alpha_{wf,ref} \left(\frac{\dot{m}_{wf}}{\dot{m}_{wf,ref}}\right)^{z} \tag{4}$$

Finally, the recuperator is also modelled on the basis of Eq. (1), but considering a single heat transfer zone. The recuperator global heat transfer coefficient is computed my means of Eq. (4).

2.1.2 Reciprocating piston expander

The volumetric expander is simulated by means of the grey-box model originally developed by Glavatskaya et Al. [25], adapted and validated for the reference reciprocating expander in a previous work of the Authors [27]. The model follows a lumped parameters approach as illustrated by the scheme shown in Fig. 5. A brief description of the implemented approach is reported, however the reader is invited to refer to [27] for a more detailed description.

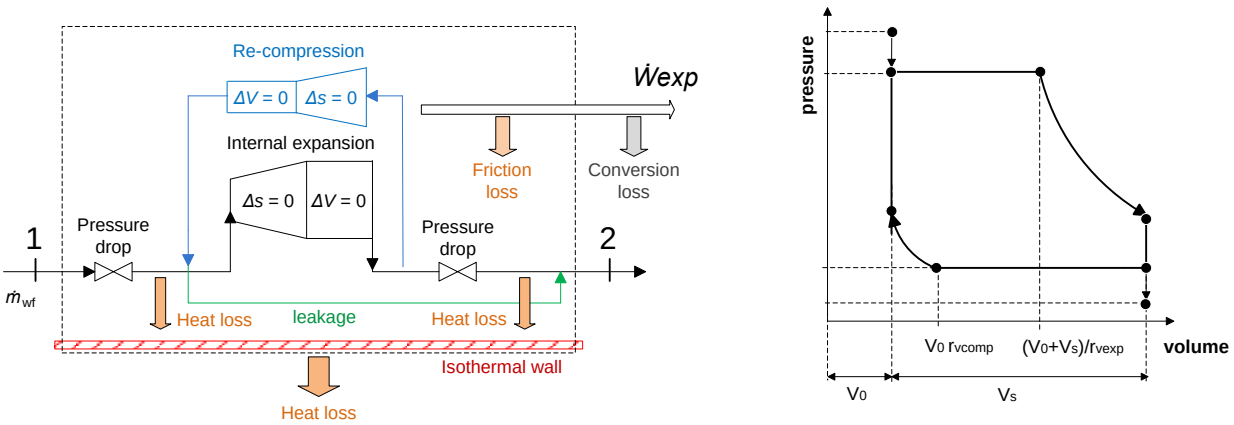

Fig. 5. The volumetric expander sub-model scheme.

The electric power output of the expander model ($\dot{W}_{exp}$) is expressed by the difference between the ideal internal expansion power, and the sum of all contributions to power losses, such as re-compression phenomena, under/over-expansion, pressure losses at inlet and outlet, internal leakages, heat dissipation, frictions and electro-mechanical conversion losses.

The expansion and the recompression transformations are modelled considering the built-in volumetric expansion and recompression ratio of the machine ($r_{v,exp}$, $r_{v,comp}$ in Tab. 1). The two volumetric ratios are used to compute the fluid state at the end of the internal expansion process, made by an isentropic followed by an isochoric transformation (see p-V diagram in Fig. 5). In a previous work of the Authors [16], the expander model has been applied to optimize the built-in volume ratio parameter, for the specific micro-ORC operating range. Therefore, in this analysis the built-in volume ratio value is chosen equal to its optimum (2.7), which allows to obtain the maximum expander power output, as demonstrated in [16].

The mass flow rate that undergoes the internal expansion is given by the difference between the flow rate entering the expander and the leakage flow. The leakage mass flow rate is calculated assuming an isentropic flow through a convergent nozzle, with a throat section area equal to the parameter A_{leak} (see Tab. 1). The mass flow rate that undergoes recompression is calculated as function of the clearance volume, parameter V_0 in Tab. 1.

The overall mechanical losses are calculated in the model by accounting for two terms: a constant term, $\dot{W}_{loss,ref}$ representing the constant mechanical loss and a second contribute, $\dot{W}_{loss,N}$ proportional to the rotational speed (see Tab. 1).

Other loss contributions are due to the pressure drop at the supply and exhaust valves and the heat dissipations through the expander walls. The supply pressure drop is modelled as the leakage mass flow, considering an isentropic expansion through a convergent nozzle, with a throat section area equal to the parameter A_{su} (see Tab. 1). The heat exchanged at the supply and exhaust section is obtained by means of the NTU method, as function of the heat transfer coefficient $(AU)_{su,ref}$, $(AU)_{ex,ref}$, parameters of the model. The heat transferred to the ambient is computed as product between the wall heat transfer coefficient ($(AU)_{amb}$ in Tab. 1) and the temperature difference between the wall and the ambient.

2.1.3 Pump and circuit resistance

The same approach proposed in [16] by the Authors is adopted in this study to model the pump behaviour within the system. According to this method, the pump operating point is determined by crossing the pump characteristic curve, at given rotational speed, and the resistance characteristic of the circuit, which depends on the number of electric loads activated.

The experimental values of the pump pressure rise as function of the volumetric flow rate are shown in Fig. 6 [16] for different values of pump rotating frequency. The "Loads" curves in figure represent the ORC circuit resistance: the increase of the expander load determines a greater hydraulic resistance of the circuit, resulting in higher values of the pressure rise for given value of volume flow rate (set by the pump frequency).

The pump and circuit resistance model allows to determine the actual pressure rise, Δp, and the volumetric flow rate, $\dot{V}$, elaborated by the pump. The mass flow rate is then obtained using the fluid density at the pump inlet. The value of η_{pp} is considered in line with experimental data [16].

$$\dot{W}_{pp} = \frac{\dot{V} \cdot \Delta p}{\eta_{pp}} \tag{5}$$

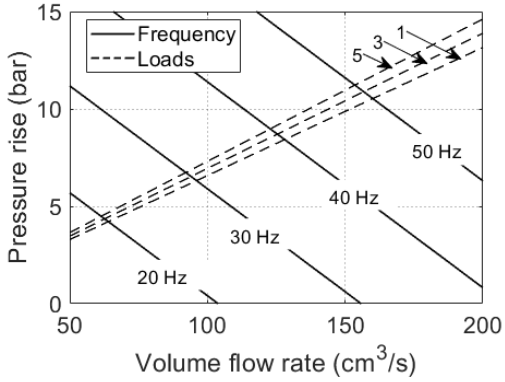

Fig. 6. ORC volumetric gear pump and circuit resistance characteristics.

2.1.4 Model validation

Before applying the ORC model to unexplored operating conditions, the model has been tested against experimental data collected during the extensive experimental campaign conducted over the reference test rig [19] using R134a, in order to evaluate the model accuracy. Results are reported in the form of parity plots, comparing main output calculated values (of evaporator thermal power, expander produced power and pump absorbed power) with the corresponding measured quantities (Fig. 7). Dashed lines are introduced in figures

to highlight different prediction error bands. Results prove the good accuracy of the model. Indeed, Fig. 7 shows that most of the parity plot points take place within the 10 % error band.

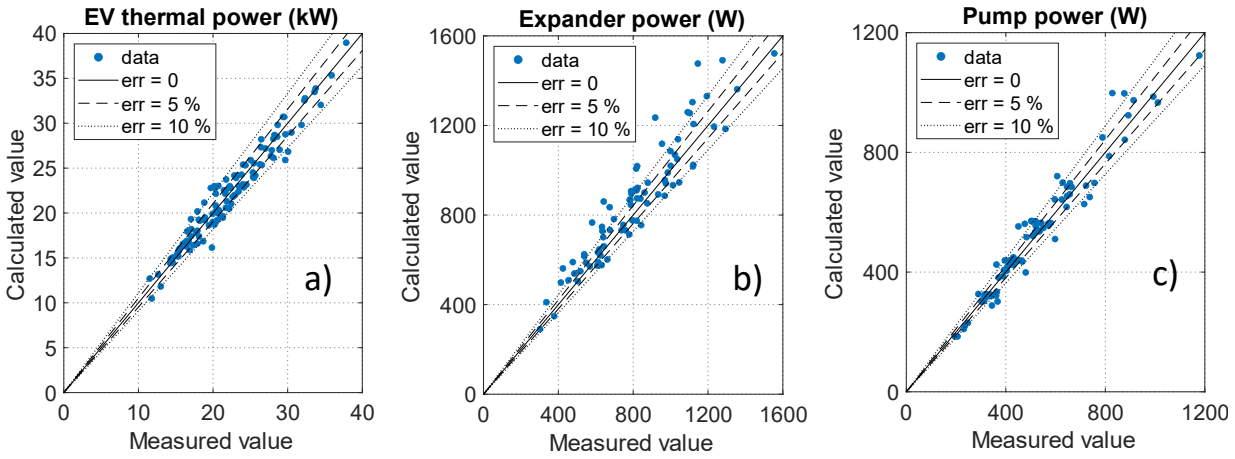

Fig. 7. Parity plot comparing calculated and measured output values: a) Evaporator thermal power; b) Expander produced electrical power; c) Pump absorbed electrical power.

2.1.5 Correction of fluid-dependent parameters

In order to cope with different working fluids, the model can be generalized, by introducing some corrections in the fluid-dependent parameters. First of all, the global heat transfer coefficients of the heat exchangers models and the expander model must be corrected. These parameters have been re-determined adopting the procedure proposed by Giuffrida [17]. The global heat transfer coefficient can be evaluated as:

$$U = \frac{Nu \cdot \lambda}{L} \tag{6}$$

where Nu is the Nusselt number and λ the conductivity, both depending on the fluid thermodynamic properties, while L represents a characteristic length determined by the component geometry. Thus, the updated global heat transfer coefficient for the new fluid, U_{new}, can be calculated as function of the reference global heat transfer coefficient, U_{ref}, and of the fluids properties, by using Eq. (7):

$$\frac{U_{new}}{U_{ref}} = \frac{Nu_{new} \cdot \lambda_{new}}{Nu_{ref} \cdot \lambda_{ref}} \tag{7}$$

In order to account for the change of the working fluid in the ORC pump and hydraulic circuit resistance model, Authors have introduced in [16] a methodology referring to volumetric pumps. According to this approach, the change of the fluid induces a change in the pump and circuit resistance curves slope. The characteristic curves, shown in Fig. 6, are updated using Eq. (8) and Eq. (9), i.e. the base equations tracing respectively the pump and the circuit resistance curves. In particular, according to Eq. (8), the volumetric flow rate elaborated by the pump, $\dot{V}$, is expressed as difference between the theoretical volumetric flow rate, $\dot{V}_{th}$, and the flow due to internal leakage, $\dot{V}_{leak}$. The $\dot{V}_{th}$ term depends on the pump geometry and rotational speed, while $\dot{V}_{leak}$ can be calculated as flow lost through the pump meatus, by means of Poiseuille's law, as a function of geometrical data, operating pressure and fluid viscosity.

$$\dot{V} = \dot{V}_{th}(geo_{pp}, N_{pp}) - \dot{V}_{leak}(geo_{pp}, \Delta p, \mu) \tag{8}$$

Eq. (9) represents the general formula for evaluating hydraulic circuit pressure head, Δp, where ε, is the equivalent flow coefficient, ρ, is the fluid density and w, the fluid velocity:

$$\Delta p = \varepsilon(geo_{circ}, n_{loads}) \cdot \rho \cdot \frac{w^2(geo_{circ}, \dot{V}, \rho)}{2} \tag{9}$$

The terms in bracket in Eqs. (8) and (9) can be indicated in explicit form and rearranged, obtaining simple relationships between Δp, $\dot{V}$, N_{pp} and n_{loads} :

$$\Delta p = (c_1 \cdot N_{pp} + c_2 \cdot \dot{V}) \cdot \mu \tag{10}$$

$$\Delta p = (c_3 \cdot n_{loads} + c_4) \cdot \dot{V} \cdot \rho \tag{11}$$

where the c_1, c_2, c_3 and c_4 coefficients are size dependent constants of the pump and of the circuit due to the geometry terms geo_{pp}, geo_{circ}; the working fluid has an impact on the equations via the fluid density, ρ, and the fluid viscosity, μ, influencing the characteristic curves slope. More details on the derivation of the relationships given above are provided in the previous paper of the Authors [16] introducing the model equations.

Thus, the model basically relies on physical/thermodynamic properties of the operating fluid and it is used here to simulate the micro ORC components main output, when run with fluids replacing the reference fluid R134a; as the substitute fluids are selected with similar properties to the replaced fluid, limited errors (in lines with the error values shown by the model in case of tests with R134a) could be expected in prediction of the new performance.

2.2 Micro-ORC global warming impact assessment

The main objective of this environmental analysis is to evaluate the total equivalent emission of CO_2 released into the atmosphere in a given operating scenario of the micro-ORC, comparing different working fluids.

The total GHG emissions from the system have been estimated by taking into account two main contributions, namely the direct emissions and the indirect emissions.

The direct emissions term, Em_{direct}, includes the environmental impact of the plant due to possible leakage of refrigerant, which occurs during system operation and servicing, and can be expressed as:

$$Em_{direct} = m \cdot LR \cdot GWP \tag{12}$$

where the main factors are: the system fluid charge m, the annual fluid leak rate LR and the fluid GWP, that is computed, in case of mixtures, as the mass weighted average of the fluid components *GWP*. The fluid charge is estimated on the basis of the internal volume of the most relevant ORC components in terms of fluid capacity, i.e. the evaporator, the condenser, the recuperator and the liquid receiver. The amount of fluid inside expander, pump and in the interconnecting pipes can be considered less relevant, considering typical internal volumes. The fluid mass enclosed in the *j*-th component could be estimated as the product between the *j*-th component volume, V_j, and the *j*-th mean fluid density, ρ_j. The mean density inside evaporator and condenser is computed as the weighted average of the densities in the different zones. The density inside the two-phase region can be calculated using Eq. (13) [28]. In particular, the volume vapour fraction γ for a generic component can be derived by the Lockhard-Martinelli model according to Liu et Al. [28], using Eqs. (14)-(16), where X_{tt} is the Martinelli parameter, x is the vapour fraction (considered equal to 0.5), μ, the fluid viscosity, and the subscripts $liquid$ and gas refer to the saturated liquid and saturated vapour fluid state respectively.

$$m_j = V_j \cdot (\rho_{liquid,j} \cdot (1 - \gamma_j) + \rho_{gas} \cdot \gamma_j) \tag{13}$$

$$X_{tt} = \left(\frac{1-x}{x}\right)^{0.9} \left(\frac{\rho_{gas}}{\rho_{liquid}}\right)^{0.5} \left(\frac{\mu_{gas}}{\mu_{liquid}}\right)^{0.1} \tag{14}$$

$$\gamma = (1 + {X_{tt}}^{0.8})^{-0.378}, \quad X_{tt} \leq 10 \tag{15}$$

$$\gamma = 0.823 - 0.157 \, ln \, X_{tt}, \quad X_{tt} > 10 \tag{16}$$

The indirect GHG emissions term ($Em_{indirect}$) considers the energy production gap (E_{gap}) as the effect of operating the micro-ORC with fluids with lower or higher thermodynamic performance than the reference fluid (R134a). Considering a constant request electric power, the energy gap needs to be supplied by a different

energy system, or it must be purchased from the electric grid. This amount of supplied energy is in general associated to an additional contribution to CO_2 emission, which depends on the emission factor (β, expressed in kilograms of CO_2 per megawatt hour of energy produced) related to the technology employed to produce the energy gap. In case the electricity is purchased from the grid, β corresponds to the average emission of the fleet of machines in the considered area of the world. Ultimately, the indirect emissions, $Em_{indirect}$, are calculated as the product between the energy gap, E_{gap}, and the emission factor, β, associated to the alternative energy provider:

$$Em_{indirect} = E_{gap} \cdot \beta \tag{17}$$

As mentioned above, the R134a is considered as baseline fluid. Thus, E_{gap} is given by the difference between the energy produced by the ORC adopting R134a as working fluid (E_{R134a}) and the energy production with the replacing fluid in exam (E_{fluid}):

$$E_{gap} = E_{R134a} - E_{fluid} \tag{18}$$

With the aim of evaluating the ORC environmental performance on a reference wide time span, all the energy terms are calculated on a yearly basis.

The complete performance model and GHG assessment procedure has been implemented in the Matlab environment [29], where, the fluids properties used to predict the micro-ORC thermodynamic conditions have been calculated by means of the REFPROP library [30].

3 Boundary conditions and performance results

3.1 Boundary conditions

The investigation on the micro-ORC system performance and its related GHG impact has been carried out under given boundary conditions, considering a certain scenario, as defined below, in terms of: i) hot source temperature and flow rate annual profiles; ii) cold source temperature and flow rate annual profiles; iii) leak rate and reference emission factor parameters. Different working fluids have been applied to the given scenario, including both pure fluids and mixtures. The selected fluids belong to the group of the most recent options of low GWP alternatives of R134a for refrigeration sector derived from the literature survey performed by Heredia-Aricapa et al. [6]. The list of considered fluids does not mean to be exhaustive, as other few options are currently available and new compounds are expected to enter the market in the next future. The goal of the analysis is rather to show the methodology and highlight some critical aspects related to the use of the most representative fluid options, but the same approach can be applied to any fluid of which thermodynamic properties are available. The selected alternative fluids are:

- R1234yf and R1234ze(E) pure fluids;
- mixture of 50 % R134a and 50 % R1234yf in mass, named in this study “R1234yf mix”;
- mixture of 50 % R134a and of 50 % R1234ze(E) in mass, named in this study “R1234ze(E) mix”;
- R515A, which consists in a mixture of 88 % R1234ze(E) and 12 % R227a in mass;
- R430A, which consists in a mixture of 76 % R152a and 24 % R600a (isobutane) in mass.

R1234yf and R1234ze(E) are the most suitable low-GWP pure HFOs for heat recovery applications at temperature lower than 100 °C (given their critical temperature close to 100 °C). Though these fluids present very similar thermodynamic properties compared to R134a (see Tab. 2), some small but not negligible differences exist, influencing the performance of the ORC components, especially in case of pump and expander of volumetric type [16]. One of the main factors of influence over the cycle performance is the expansion pressure ratio, which depends on the pressures at which the fluid evaporates and condenses into the cycle at given temperatures of the hot and cold source respectively. Other properties that can have an impact on performance and internal losses of the volumetric machines are the density and the viscosity of the fluid.

Beside the GWP issue, another fundamental aspect to consider is the fluid safety and flammability in particular. Most of HFO fluids have the disadvantage of being classified A2L, according to ASHRAE Standard

34, i.e. mildly flammable refrigerant category (this A2L class applies to R1234yf and R1234ze(E), see Tab. 2). This feature may not always be constrictive in the working fluid selection for refrigeration applications, but it should be taken into account in the ORC applications, where the operating temperature range is higher and flammability risk of the fluid could increase. Options to decrease the flammability risk while containing the GWP issue at the same time, rely on blending the HFOs with non-flammable fluids with similar thermodynamic properties, such as the basic R134a (classified as A1, i.e. non-flammable, according to ASHRAE). Thus the "R1234yf mix" and "R1234ze(E) mix" cases have been considered in the study, as intermediate mid-term options for the replacement of the R134a. In addition, two blends have been considered in the comparison: the azeotropic binary mixture with commercial name R515A (R234ze(E) and R227) (classified as A1), , and the near azeotropic blend composed of R152a and R600a, named R430A, which is a mixture often indicated in literature as a potential good candidate for R134a replacement in refrigeration application [6]. R430A exhibits favorable properties, as highlighted in Tab. 2, such as: i) lower GWP in comparison with R134a and the other mixtures containing HFCs; ii) lower densities and viscosities compared to the other analysed fluids; iii) higher latent heat of vaporization values at given temperature (see Tab. 2, Δh_{sat} (60 °C)), which influence the heat transfer performance of the evaporator and of the condenser. Nevertheless, it should be highlighted that this fluid mixture has a high-flammability classification (A3), as it contains a HC compound (R600a).

Tab. 2. Main characteristics of the analysed pure fluids and binary mixtures (properties obtained with REFPROP [30], GWP values from IPCC AR5 [32])

Properties	**Fluid name and type**						
	R134a	**R1234yf**	**R1234ze(E)**	**R1234yf mix**	**R1234ze(E) mix**	**R515A**	**R430A**
Composition	Pure fluid	Pure fluid	Pure fluid	50% R134a / 50% R1234yf in mass	50% R134a / 50% R1234ze(E) in mass	88 % R1234ze(E) / 12 % R227a in mass	76 % R152a / 24 % R600a in mass
$T_{critical}$ (°C)	101.1	94.7	109.4	95.3	103.8	108.7	107.0
p_{sat} (@ 25 °C) (bar)	6.7	6.8	5.0	7.1	6.0	4.9	6.5
$p_{sat,liquid}$ (@ 60 °C) (bar)	16.8	16.4	12.8	17.4	15.2	12.7	15.7
Δh_{sat} (@ 60 °C) (kJ/kg)	139.1	110.4	135.5	120.4	135.4	128.8	218.4
$\rho_{sat,liquid}$ (@ 25 °C) (kg/m^3)	1207	1092	1163	1141	1181	1187	760
$\rho_{sat,gas}$ (@ 60 °C) (kg/m^3)	87.4	99.8	70.1	99.7	80.7	72.5	50.3
$\mu_{sat,liquid}$ (@ 25 °C) (Pa·s) · 10^4	1.95	1.53	1.90	1.68	1.90	1.94	1.43
GWP (-)	1300	1	1	650.5	650.5	403	106
ASHRAE class	A1 [6]	A2L [31]	A2L [31]	A1 [33]	A1 [33]	A1 [6]	A3 [6]

Regarding the operating scenario of the micro-ORC, in order to determine the final energy production and GHG emissions of the system, a yearly operating cycle can be taken into account, for what concern: i) the hot source temperature and flow rate profiles; ii) the cold source temperature and flow rate profiles. The case study of a real geothermal application with a micro-ORC installed at a swimming pool centre [22] has been investigated in this study; the same approach can be applied to ORC operated with different heat sources, profiles and time horizons. The heat source consists in a geothermal well that supplies liquid water at a barely constant temperature close to 60 °C, with a volume flow rate of 22 m^3/h. The cold water sink is the swimming pool heating circuit, with inlet water temperature nearly equal to 18 °C an average volume flow rate of 25 m^3/h; because of the negligible dependency of the water temperature on the ambient conditions, the latter is considered constant during the year. The ORC pump frequency value is adjusted to maintain the evaporating pressure that assures the maximum ORC net power output, at the given boundary conditions. A minimum superheating degree of 3 °C is imposed as constraint, in order to avoid wet expansion. Thus, a different optimal pump frequency value is considered for the ORC when using different fluids. The subcooling degree is chosen constant and equal to 4 ° C, according to the subcooling degree value observed experimentally. Finally, 5 activated loads absorbing the expander power output are considered, to receive electric power up to 3 kW.

3.2 Performance results

The main indexes of interest for the analysis are compared by means of the radar plot in Fig. 8; they comprise: i) the expander electric power output ($\dot{W}_{exp}$); ii) the pump absorbed electric power ($\dot{W}_{pp}$); iii) the evaporator input thermal power ($\dot{Q}_{ev}$); iv) the ORC net efficiency (η_{net}); v) and the fluid global warming potential (GWP). ORC net efficiency is computed by means of Eq. (19).

$$\eta_{net} = \frac{\dot{W}_{exp} - \dot{W}_{pp}}{\dot{Q}_{ev}} \tag{19}$$

Other operating conditions, such as the feed-pump frequency, the working fluid flow rate, the superheating degree, the evaporating and condensing pressure and their ratio are reported in Tab. 3.

When comparing R134a with the other fluids containing HFOs, results show that the most performing fluid is the reference fluid, R134a (see Fig. 8a). Indeed, it provides the maximum power production (1485 W) and the best net efficiency (7.5 %). R1234yf, among the pure fluids, has the closest performance to R134a. It exhibits a lower expander power output (-22%), but similar pump power consumption (about 390 W). Main factors determining the performance drop introduced using HFO fluids can be identified in: (i) the lower pressure ratio (leading to smaller enthalpy drop available across the expander); (ii) the lower viscosity (mainly affecting the leakage losses at the pump meatus and thus the elaborated mass flow rate, for more detail refer to [16]). The less performing fluid is R515A, showing both lower power (-38%) and lower pump consumption, but also lower net efficiency (a reduction close to 1%). The energy performance of R1234ze(E) are comparable to the ones of R515A, due to their very similar composition. Hence, the olefine R1234ze(E) is preferable to its blend with R227a, since the pure fluid presents lower GWP value (6 for R1234ze(E) vs 387 for R515A), unless flammability is an issue to be considered in the specific installation. The overall performance obtained with R1234yf mix and R1234ze(E) mix are intermediate between the ones of the two composing pure fluids; in comparison with R515A, these two HFO/HFC mixtures provide higher efficiency values, but are also characterized by higher GWP.

Comparison between R430A and R134a (see Fig. 8b) shows instead that higher performance can be achieved with the substitute fluid. The net electric efficiency increases of more than 1%, while the electric power output significantly rises (up to almost 2.4 kW – 60 % increment). This is mainly imputable to the higher enthalpy drop available at the expander (21 kJ/kg against 15 kJ/kg), but also to the better heat transfer properties the R430A, which allows to recover a large amount of heat at the evaporator for a given available hot source temperature and flow rate and given the ORC components size. Indeed, the calculated $\dot{Q}_{ev}$ value in case of R430A is almost 3/2 of the reference value (it is equal to 21 kW vs 15 kW in case of R134a case). Similar organic fluid flow rate values for R430A and R134a cases (83 g/s and 91 g/s, respectively, see Tab. 3) have been obtained, as function of the operating pressure and densities and the geometric characteristics of the circuit, according to the model described in the previous paragraphs. The comparison shows that R430A provides for approximately a 1/10 reduction in GWP, but also for a high flammability risk (it is the only considered fluid with A3 classification), which requires a careful analysis before applying it to an ORC system.

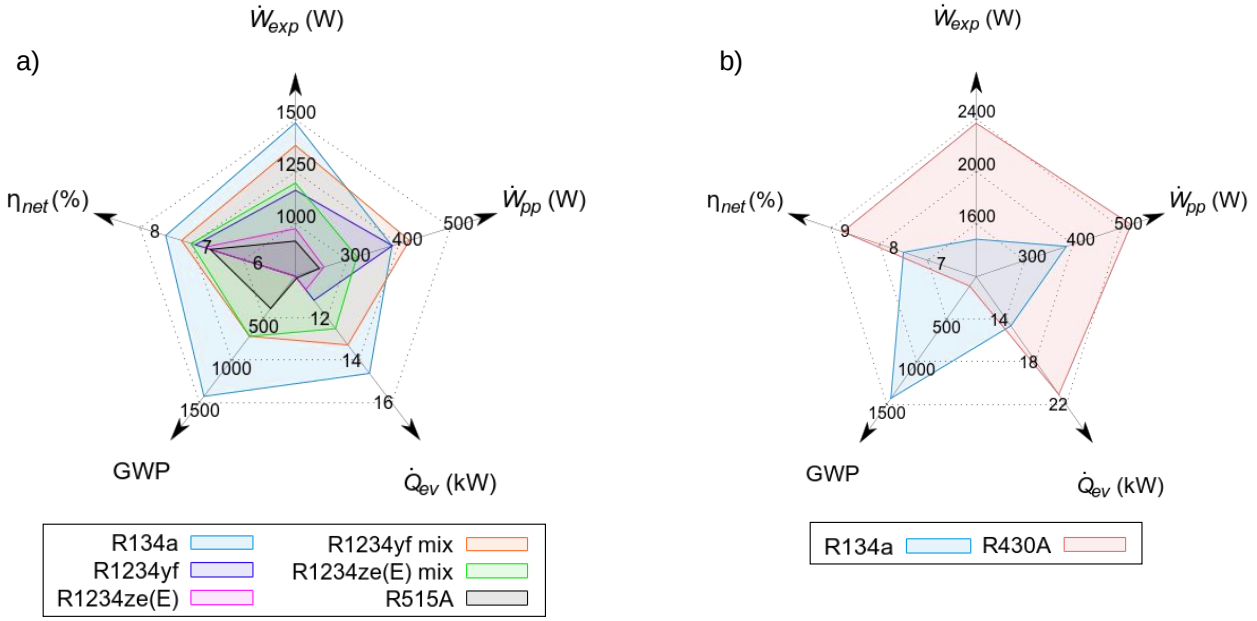

Fig. 8. Micro-ORC system and components performance: a) comparison of R134a with HFO-based fluids; b) comparison of R134a with R430A.

Tab. 3. Micro-ORC system thermodynamic operating conditions – fluids comparison.

Parameters \ Fluids	R134a	R1234yf	R1234ze(E)	R1234yf mix	R1234ze(E) mix	R515A	R430A
Pump frequency, f_{pp} (Hz)	28	31	22	31	25	21	37
Working fluid flow rate, $\dot{m}_{wf}$ (g/s)	91.4	86.1	70.0	92.8	80.5	69.5	82.9
Superheating degree (°C)	3	3	3	3	3	3	3
Evaporating pressure (bar)	15.6	15.3	11.8	16.2	13.9	14.6	11.7
Condensing pressure (bar)	7.5	7.7	6.5	7.8	7.0	7.4	6.4
Pressure ratio (-)	2.08	1.98	1.82	2.09	2.00	1.96	1.82

The yearly electric energy production in the considered operating scenario is provided in Tab. 4 for the different fluids. Indirect and direct GHG emissions (via Eqs. (17) and (12)) are affected by two key quantities, also shown in Tab. 4: the yearly electric energy gap (E_{gap}) and the fluid charged in the system (m).

The R134a base case fluid shows a yearly net electric energy production value (9621 kWh), larger than the values obtained with the HFO/HFC blends; the decrease is about 13 % and 20 %, respectively for the R1234yf mix and the R1234ze(E) mix; a decrease of about 12 %, 18 % and 24 % is obtained respectively with R1234yf, R1234ze(E) and R515A. R134a yearly energy production has been considered as reference (E_{R134a}), when applying Eq. (18), in order to compute the E_{gap} value. The highest E_{gap} value is calculated in case of R515A. On the contrary, R430A presents a negative E_{gap} value, because of its better performance with respect to the R134a case.

The calculated value of the fluid charge, for the ORC operating with R134a, is equal to 28.8 kg, which is in line with experimental experience over the reference test bench [19]. Fluid charge values for the other fluids are slightly different, because of the different ORC thermodynamic setup (see Tab. 3) and due to different values of density of the fluids (see Tab. 2), according to Eqs. (13-16). As expected, the lowest value regards the case of R430a, with fluid charge of 20.5 kg, 40% less than R134a.

Tab. 4. ORC energy performance and fluid charge, affecting GHG emissions assessment – fluids comparison.

Parameters \ Fluids	R134a	R1234yf	R1234ze(E)	R1234yf mix	R1234ze(E) mix	R515A	R430A
Yearly net electric energy, E (kWh)	9621	6777	6323	8378	7684	5876	16182
Yearly electric energy gap, E_{gap} (kWh) $(E_{gap} = E_{R134a} - E_{fluid})$	0	2843	3298	1243	1937	3745	-6562
Working fluid charge, m (kg)	28.8	27.4	27.1	28.9	28.5	27.1	20.5

4 Environmental impact assessment

The environmental impact of the micro-ORC system is firstly evaluated for a reference case study, assuming:

- A leak rate equal to 2 % as characteristic value provided for Residential and Commercial A/C, including Heat Pumps, by IPCC Good Practice Guidelines and Uncertainty Management in National Greenhouse Gas Inventories (2000) [34];
- An emission factor of the energy provider (β) equal to 460 $kgCO_2/MWh$, corresponding to the average EU-27 emission factor according to [35].

However, in order to provide more general and comprehensive results, a parametric analysis has been conducted by varying the leak rate and the emission factor values are proposed. Furthermore, an additional sensitivity analysis concerning the influence of the concentration of R134a into the R134a/HFO mixtures is presented. Results of the GHG impact assessment are presented in terms of specific direct, indirect and total yearly equivalent CO_2 emissions. Specific emissions are here expressed per unit of produced electric energy (E).

The calculated specific emissions of the micro-ORC system, when working with the different fluids, are provided in the bar plot of Fig. 9. As first important result, it must be observed that HFOs and their mixtures do not reduce the overall CO_2 equivalent emissions, even if the direct emission contribution related with GWP is reduced. Actually, the use of R1234yf increases the total specific emission by 148 % and R1234ze(E) even by 208 %. The two mixtures with HFOs and R134a exhibits intermediate values of total emission, compared to the pure fluids composing the mixtures. Total emissions related to the use of pure R134a are associated to only direct emissions, equal to 78 $kgCO_2/MWh$. Conversely, total emissions related to the use of pure HFOs are basically due to the indirect emission term, since the direct emissions contribution is almost negligible (about 0.08 $kgCO_2/MWh$) due to the associated low GWP values.

The R515A case leads to the highest specific emission, up to 330 $kgCO_2/MWh$, due to the remarkable contribution of the indirect term and to the not negligible fluid GWP value. As shown in Fig. 9, the R430A mixture would provide at the same time: 1) a limited direct GHG emission term, due to the reduced GWP in comparison with R134a, and 2) a negative indirect emission term, due to improved energy performance (negative energy gap), resulting in a net gain in total equivalent CO_2 emission.

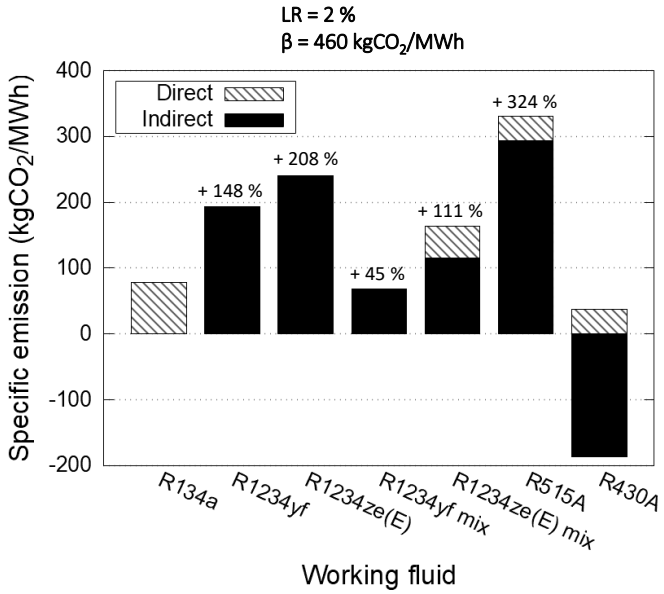

Fig. 9. CO_2 equivalent emissions – fluids comparison (percentage values are related to R134a total emissions).

The outcome described above is valid when considering an annual leak rate equal to 2%. Indeed, direct emissions scale up proportionally to the leak rate, and at higher *LR* values the direct contribution becomes more decisive than the indirect one. Values of the leak rate up to 15% have been explored; higher leak rate instead would not be realistic since representative of large centralized systems (17 % for example represents the typical annual leak rate associated to Centralized Supermarket Refrigeration Systems [34]). Parametric analysis demonstrates that emissions are quite sensitive to the leak rate (see Fig. 10) and the sensitivity (i.e. the curve slope) increases in particular with the fluid GWP. For instance, for the R134a case, specific emission at *LR* = 15 % are more than seven times the specific emission at *LR* = 2%. On the other hand, specific emissions for the HFOs pure fluids remain almost constant by varying the leak rate, because the direct contribution does not change significantly. It must be noticed that, in most of the cases, the R134a specific emission curve crosses the HFOs' one around a leak rate value of 5 %, which can represent a so called "inversion point". Above the inversion point, the R134a specific emission becomes higher than the HFO's ones and the considerations made for *LR* = 2 % are no more valid. For what concerns R515A, this "inversion point" is shifted at around *LR* = 14 %. In general terms, knowing the actual annual leak rate of the system is of utmost importance in order to perform a correct evaluation of the global warming impact of the micro-ORC.

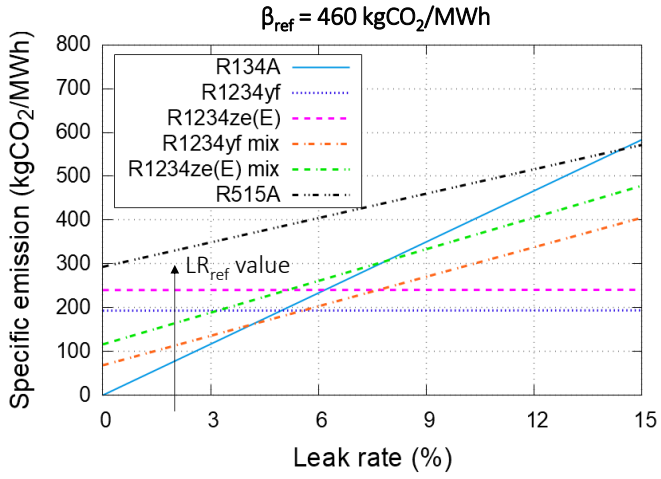

Fig. 10. CO_2 equivalent emissions as function of the leak rate – fluids comparison.

Another factor of influence is the reference emission factor β (see Eq (17)), which depends on the energy mix providing the energy gap. A parametric study has been performed (Fig. 11), exploring β values ranging

between the lowest (23 $kgCO_2/MWh$ - Sweden) and the highest (1191 $kgCO_2/MWh$ - Poland) emission factor values documented among the EU-27 countries [35]. It must be noticed that over almost all the explored β range, the specific emissions are higher for all the analysed fluids compared to R134a, as shown in Fig. 11. In particular, higher β values lead to higher indirect emissions and could discourage the use of low-GWP fluids and mixtures even more, as alternatives of R134a. It can be observed that in this sensitivity analysis the R134a specific emission remain constant versus β, whilst the emissions for the fluids containing HFOs vary proportionally to β, with a curve slope determined by the E_{gap} value. The relative deviation from the reference value of β (shown in the figure) ranges between -88 % to +159 % for the HFOs pure fluids.

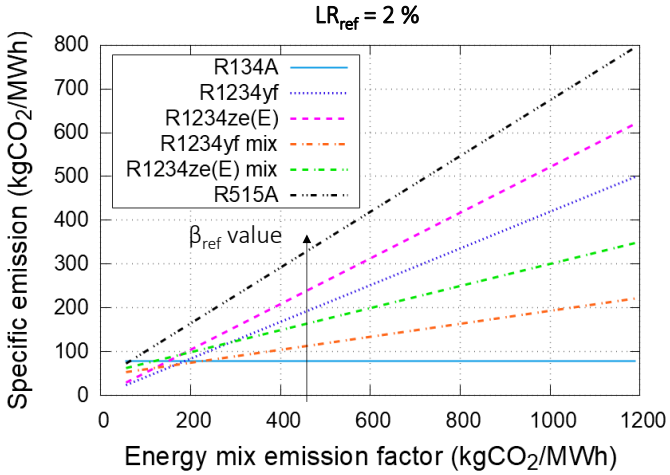

Fig. 11. CO_2 equivalent emissions as function of the energy mix emission factor – fluids comparison.

Coming back to the reference case (β = 460 $kgCO_2/MWh$ and LR = 2%), a further discussion is finally proposed, investigating the effect of R134a fraction within mixtures based on HFOs. In particular, Fig. 12a shows the influence of the R134a concentration on the total specific GHG micro-ORC emissions, in variable mixtures of R1234yf with R134a, and mixtures of R1234ze(E) with R134a. The extreme conditions with R134a concentration equal 0 % and 100 % indicate respectively, HFO and R134a pure fluid. Among the possible mixtures it must be cited the commercial mixture R513A [31] (composed by 44% of R134a and 56% R1234yf) highlighted for convenience in Fig. 12b.

The Em_{direct} term increases almost linearly with R134a amount in the mixture, due to the higher GWP of R134a than HFOs (see Tab. 2). The trend is not strictly linear because of the different required fluid charge, influencing the actual annual fluid leakage. Trends for R1234yf mixture and R1234ze(E) mixture are very similar because of the similar GWP of R1234yf and R1234ze(E) pure fluids. The $Em_{indirect}$ term exhibits a trend opposite to the Em_{direct} term. Indeed, increasing the R134a concentration leads to better performance of the micro-ORC systems and thus to lower need of energy integration and to lower $Em_{indirect}$. The mixture of R134a with R1234yf shows better performance than the mixture of R134a with R1234ze(E), and in particular lower $Em_{indirect}$ at given R134a concentration. The sum of the direct and indirect emissions contributions gives the total emission trend reported in Fig. 12b.

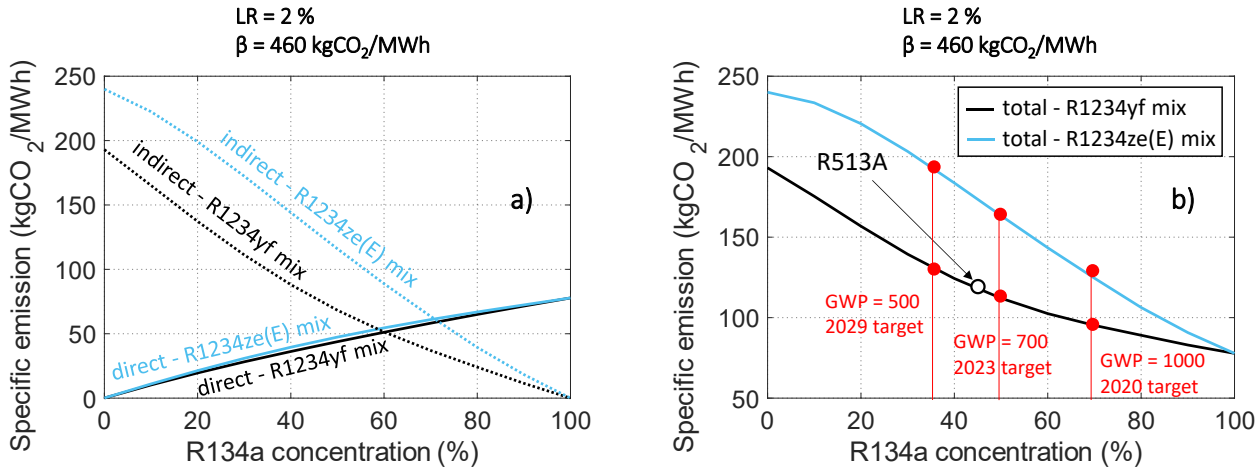

Fig. 12. CO_2 Specific emission as function of R134a concentration in the mixture: a) direct and indirect contributions; b) total specific emission.

Maps of the specific emission as function of the emission factor and of the R134a concentration are reported in Fig. 13. Dotted line in Fig. 13 indicates the reference total emission observed using R134a pure fluid (equal to 78 $kgCO_2/MWh$ (see Fig. 12a)) considering the reference emission factor equal to 460 $kgCO_2/MWh$.

On the basis of the expected HFCs phase-down timeline, average GWP of refrigerants on the market should gradually reduce in next years (as indicated in Fig. 1). As a consequence, R134a should has been withdrawing from the market starting from year 2020, and the R134a concentration in the mixtures of R134a and HFOs should decrease in the following years (as indicated Fig. 12b). Maps of Fig. 13 gives an indication on how the emission factor should be reduced hand-in-hand with the R134a reduction in the mixtures, in order to contain total emission related to the use of refrigerants. To the same aim, energy mix emission factor should decrease from 460 $kgCO_2/MWh$ to less than 200 $kgCO_2/MWh$ in about ten years. A similar reduction could be achieved only in the case where the countries energy mix will be overturned. Indeed, nowadays, just a few European countries fall under emission factor below 200 $kgCO_2/MWh$, among which are France (56 $kgCO_2/MWh$) and Sweden (23 $kgCO_2/MWh$) mainly thanks to their large nuclear fleet [36].

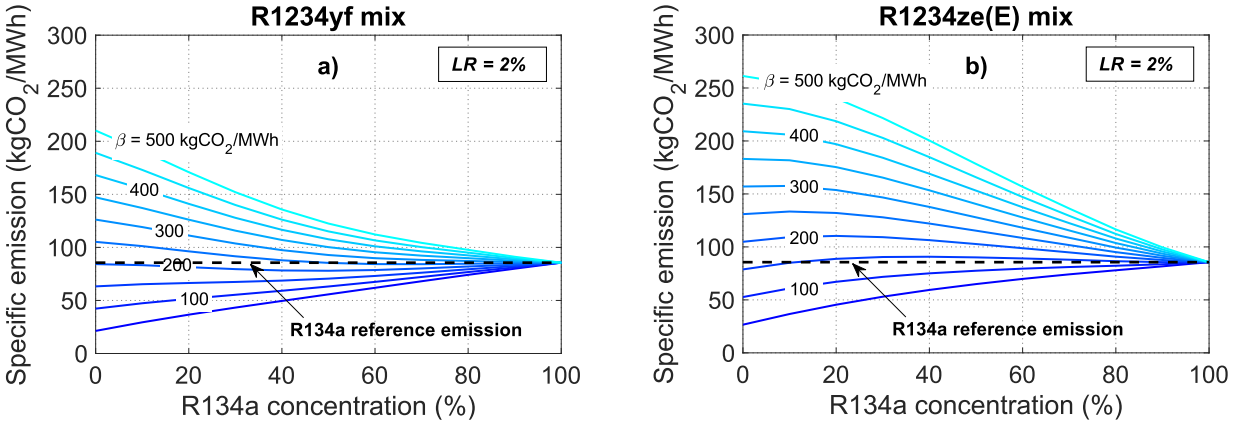

Fig. 13. Maps of the specific emission as function of the emission factor and the R134a concentration, for: a) mixture of R134a and R1234yf; b) mixture of R134a and R1234ze(E).

This final analysis intends to highlight how combined actions could be requested in order to effectively reduce emissions related to systems using refrigerants as working fluids, such as micro-ORC: i) the decrease of working fluids GWP, to limit direct emissions; ii) a reduction of the energy mix emission factor, in order to contain possible indirect emissions. With a view to move towards a greener energy mix, emissions factors are expected to decrease in next years and the use of low GWP fluids could help to effectively reduce GHG emissions. Meanwhile, in this transition period, blends of R134a and HFOs could help to maintain limited indirect emissions, while respecting new regulation concerning high GWP refrigerants (see Fig. 9).

Conclusion

This paper presented a novel methodology for the assessment of the total warming impact due to the working fluids adopted in ORC for low-grade heat recovery. A reference case regarding the hydrofluorocarbon (HFC) R134a, employed in a micro-ORC system, is compared numerically with some of its potential replacement fluids with lower global warming potential (GWP). The alternative fluids considered in this analysis are two pure hydrofluoroolefines (HFOs - R1234yf and R1234ze(E)), and four mixtures (R134a-R1234yf; R-134a-R1234ze(E); R515A; R430A). In addition to the evaluation of the direct CO_2 emissions, based on the GWP and on the leak rate of the working fluids, an indirect contribution of emission has been included in the analysis. This contribution accounts for the emissions due to the use of fluids with lower performance than R134a, requiring an additional amount of electricity, to which an emission factor is associated. The aim was to establish the real potential of low-GWP fluids and their blends with R134a, in reducing the greenhouse gases release compared to conventional HFC. For this purpose, a robust semi-empirical model of the whole micro-ORC system is applied, to account for the actual operation of the cycle, including the real performance of the volumetric expander and pump. Some modifications to the original model equations have been introduced, to account for the change of fluid properties.

The results of the comparison reveal that HFO fluids, characterized by very low value of GWP, are related in general to a decrease of performance with respect to R134a. Thus, HFOs and their mixtures introduce a gap of energy production, which must be compensated with alternative energy sources, or purchased from the grid. Considering an annual leak rate equal to 2%, indirect emissions caused by the use of HFOs determine total equivalent CO_2 emissions greater than those related to R134a, up to + 208% by employing R1234ze(E). Among the examined fluids only the case of the mixture named R430a leads to a substantial reduction of the total warming impact, since this fluid presents higher performance and lower GWP than R134a. On the contrary, R430a is considered at high risk of flammability, hence its application in ORC systems requires careful evaluation.

A parametric analysis by varying the annual leak rate highlights that emissions are quite sensitive to the leak rate. Thus, knowing the actual annual leak rate of the system is important in order to perform a correct evaluation of the greenhouse impact. Unfortunately, specific data for small scale ORC are scarce and not available. Further research could be dedicated to collect data concerning annual leak rate of this kind of plants. Other factor of influence is the emission factor of the energy mix considered to provide the energy production gap. It must be noticed, indeed, that higher emissions factors lead to higher indirect emissions and could discourage the use of low GWP as alternatives of R134a. Anyway, recent energy targets intend to push toward greener energy mix, emissions factors are expected to decrease and the use of low-GWP fluids may help to effectively reduce greenhouse gas emissions. At least, blends exhibit, as expected, intermediate emissions compared to pure fluids forming the mixture, and also intermediate performance. Hence, in this transition period, they could help to maintain a good trade-off between performance and greenhouse impact.

In conclusion, this study turns the attention on how combined actions are requested in order to effectively reduce emissions related to systems using refrigerants as working fluids, such as micro-ORC. The decrease of the GWP of working fluids, limiting direct emissions must be accompanied by a substantial reduction of the energy mix emission factor, in order to contain possible indirect emissions.

Nomenclature

Symbols

A	Area	(m^2)
α	Convective heat transfer coefficient	($W/m^2/K$)
β	Emission factor	($kgCO_2/MWh$)
Δ	Difference	(-)
E	Energy	(MWh)
Em	Emission	($kgCO_2$)
ε	Flow coefficient	(-)
γ	Void fraction	(-)
f_{pp}	Pump feed frequency	(Hz)
L	Length	(m)
LR	Leak rate	(-)
λ	Conductive heat transfer coefficient	(W/m/K)
m	Mass	(kg)
$\dot{m}$	Mass flow rate	(kg/s)
μ	Viscosity	(Pa·s)
N	Rotating speed	(rpm)
Nu	Nusselt number	(-)
n_{loads}	Numbers of activated loads	(-)
η	Efficiency	(-)
p	Pressure	(bar)
ρ	Density	(kg/m^3)
$\dot{Q}$	Thermal power	(W)
r_v	Built-in volume ratio	(-)
s	Entropy	(kJ/kg/K)
T	Temperature	(°C)
U	Global heat transfer coefficient	($W/m^2/K$)
V	Volume	(m^3)
$\dot{V}$	Volumetric flow rate	(m^3/s)
$\dot{W}$	Electrical power	(W)
w	Velocity	(m/s)
x	Vapour fraction	(-)
X_{tt}	Martinelli parameter	(-)
c, z, y	Constants	

Abbreviations

CD	Condenser
COMP	Compression
EV	Evaporator
EXP	Expander
geo	Geometry
PP	Pump
REC	Recuperator
RES	Circuit resistance

Subscripts

amb	Ambient
circ	Circuit
H_2O	Water
leak	Leakage
log	Logarithmic
ref	Reference
sat	Saturation
sc	Subcooling
sh	Superheating
su	Supply
th	Theoretical
tp	Two-phase
wf	Working fluid

Acronyms

GHG	Greenhouse Gas
GWP	Global Warming Potential
HC	HydroCarbon
HFC	HydroFluoroCarbon
HFO	HydroFluoroOlefine
ORC	Organic Rankine Cycle

References

1. 2030 Climate & Energy Framework Available online: https://ec.europa.eu/clima/policies/strategies/2030_en (accessed on 28 April 2020).
2. Tocci, L.; Pal, T.; Pesmazoglou, I.; Franchetti, B. Small Scale Organic Rankine Cycle (ORC): A Techno-Economic Review. *Energies* **2017**, *10*, 413, doi:10.3390/en10040413.
3. Park, B.-S.; Usman, M.; Imran, M.; Pesyridis, A. Review of Organic Rankine Cycle Experimental Data Trends. *Energy Convers. Manag.* **2018**, *173*, 679–691, doi:10.1016/j.enconman.2018.07.097.
4. IPCC, 2013: Climate Change 2013: The Physical Science Basis. Contribution of Working Group I to the Fifth Assessment Report of the Intergovernmental Panel on Climate Change I (Chapter 8, Appendix 8.A), https://www.ipcc.ch/site/assets/uploads/2018/02/WG1AR5_Chapter08_FINAL.pdf
5. Regulation (EU) No 517/2014 of the European Parliament and of the Council of 16 April 2014 on fluorinated greenhouse gases and repealing Regulation (EC) No 842/2006 Text with EEA relevance, http://data.europa.eu/eli/reg/2014/517/oj
6. Heredia-Aricapa, Y.; Belman-Flores, J.M.; Mota-Babiloni, A.; Serrano-Arellano, J.; García-Pabón, J.J. Overview of Low GWP Mixtures for the Replacement of HFC Refrigerants: R134a, R404A and R410A. *Int. J. Refrig.* **2020**, *111*, 113–123, doi:10.1016/j.ijrefrig.2019.11.012.
7. Zilio, C.; Brown, J.S.; Schiochet, G.; Cavallini, A. The Refrigerant R1234yf in Air Conditioning Systems. *Energy* **2011**, *36*, 6110–6120, doi:10.1016/j.energy.2011.08.002.
8. Lee, Y.; Jung, D. A Brief Performance Comparison of R1234yf and R134a in a Bench Tester for Automobile Applications. *Appl. Therm. Eng.* **2012**, *35*, 240–242, doi:10.1016/j.applthermaleng.2011.09.004.

9. Zhao, Y.; Qi, Z.; Chen, J.; Xu, B.; He, B. Experimental Analysis of the Low-GWP Refrigerant R1234yf as a Drop-in Replacement for R134a in a Typical Mobile Air Conditioning System. Proceedings of the Institution of Mechanical Engineers, Part C: Journal of Mechanical Engineering Science 2012, 226, 2713–2725, doi:10.1177/0954406211435583.
10. Mota-Babiloni, A.; Navarro-Esbrí, J.; Barragán, Á.; Molés, F.; Peris, B. Drop-in Energy Performance Evaluation of R1234yf and R1234ze(E) in a Vapor Compression System as R134a Replacements. *Appl. Therm. Eng.* **2014**, *71*, 259–265, doi:10.1016/j.applthermaleng.2014.06.056.
11. Invernizzi, C.M.; Iora, P.; Preißinger, M.; Manzolini, G. HFOs as Substitute for R-134a as Working Fluids in ORC Power Plants: A Thermodynamic Assessment and Thermal Stability Analysis. *Appl. Therm. Eng.* **2016**, *103*, 790–797, doi:10.1016/j.applthermaleng.2016.04.101.
12. Boyaghchi, F.A.; Chavoshi, M.; Sabeti, V. Optimization of a Novel Combined Cooling, Heating and Power Cycle Driven by Geothermal and Solar Energies Using the Water/CuO (Copper Oxide) Nanofluid. *Energy* **2015**, *91*, 685–699, doi:10.1016/j.energy.2015.08.082.
13. Molés, F.; Navarro-Esbrí, J.; Peris, B.; Mota-Babiloni, A.; Mateu-Royo, C. R1234yf and R1234ze as Alternatives to R134a in Organic Rankine Cycles for Low Temperature Heat Sources. *Energy Procedia* **2017**, *142*, 1192–1198, doi:10.1016/j.egypro.2017.12.380.
14. Yamada, N.; Mohamad, M.N.A.; Kien, T.T. Study on Thermal Efficiency of Low- to Medium-Temperature Organic Rankine Cycles Using HFO−1234yf. *Renew. Energy* **2012**, *41*, 368–375, doi:10.1016/j.renene.2011.11.028.
15. Le, V.L.; Feidt, M.; Kheiri, A.; Pelloux-Prayer, S. Performance Optimization of Low-Temperature Power Generation by Supercritical ORCs (Organic Rankine Cycles) Using Low GWP (Global Warming Potential) Working Fluids. *Energy* **2014**, *67*, 513–526, doi:10.1016/j.energy.2013.12.027.
16. Bianchi M, Branchini L, De Pascale A, Melino F, Ottaviano S, Peretto A, Torricelli N. Replacement of R134a with low-GWP fluids in a kW-size reciprocating piston expander: performance prediction and design optimization. Energy Vol. 206, 1 September 2020, 118174. https://doi.org/10.1016/j.energy.2020.118174.
17. Giuffrida, A. Modelling the Performance of a Scroll Expander for Small Organic Rankine Cycles When Changing the Working Fluid. *Appl. Therm. Eng.* **2014**, *70*, 1040–1049, doi:10.1016/j.applthermaleng.2014.06.004.
18. Andreasen, J. G., Larsen, U., Knudsen, T., Pierobon, L., & Haglind, F. (2014). Selection and optimization of pure and mixed working fluids for low grade heat utilization using organic Rankine cycles. Energy, 73, 204–213. https://doi.org/10.1016/j.energy.2014.06.012.
19. Bianchi, M.; Branchini, L.; Casari, N.; De Pascale, A.; Melino, F.; Ottaviano, S.; Pinelli, M.; Spina, P.R.; Suman, A. Experimental Analysis of a Micro-ORC Driven by Piston Expander for Low-Grade Heat Recovery. *Appl. Therm. Eng.* **2019**, *148*, 1278–1291, doi:10.1016/j.applthermaleng.2018.12.019.
20. Zampieri, G. "Closed-Cycle Plant" U.S. Patent US2016/0032786A1, Feb. 4, 2016 2016.
21. Dickes, R.; Dumont, O.; Daccord, R.; Quoilin, S.; Lemort, V. Modelling of Organic Rankine Cycle Power Systems in Off-Design Conditions: An Experimentally-Validated Comparative Study. *Energy* **2017**, *123*, 710–727, doi:10.1016/j.energy.2017.01.130.
22. Bianchi, M.; Branchini, L.; De Pascale, A.; Melino, F.; Ottaviano, S.; Peretto, A.; Torricelli, N.; Zampieri, G. Performance and Operation of Micro-ORC Energy System Using Geothermal Heat Source. *Energy Procedia* **2018**, *148*, 384–391, doi:10.1016/j.egypro.2018.08.099.
23. Ziviani, D.; Dickes, R.; Lemort, V.; Groll, J.E.B. and E.A. Effects of the Working Fluid Charge in Organic Rankine Cycle Power Systems: Numerical and Experimental Analyses. *Org. Rank. Cycle Technol. Heat Recovery* **2018**, doi:10.5772/intechopen.78026.
24. *A-to-Z Guide to Thermodynamics, Heat and Mass Transfer, and Fluids Engineering: AtoZ*; Begellhouse, 2006; Vol. F;
25. Glavatskaya, Y.; Podevin, P.; Lemort, V.; Shonda, O.; Descombes, G. Reciprocating Expander for an Exhaust Heat Recovery Rankine Cycle for a Passenger Car Application. *Energies* **2012**, *5*, 1751–1765, doi:10.3390/en5061751.
26. R. Dickes, O. Dumont, R. Daccord, S. Quoilin, and V. Lemort, "Modelling of organic Rankine cycle power systems in off-design conditions: An experimentally-validated comparative study," Energy, vol. 123, pp. 710–727, Mar. 2017, doi: 10.1016/j.energy.2017.01.130.
27. Bianchi, M.; Branchini, L.; De Pascale, A.; Melino, F.; Ottaviano, S.; Peretto, A.; Torricelli, N. Application and Comparison of Semi-Empirical Models for Performance Prediction of a KW-Size Reciprocating Piston Expander. *Appl. Energy* **2019**, *249*, 143–156, doi:10.1016/j.apenergy.2019.04.070.
28. Liu, L.; Ma, J.; Zhu, T. Working Fluid Charge Oriented Off-Design Modeling of a Small Scale Organic Rankine Cycle System. *Energy Convers. Manag.* **2017**, *148*, 944–953, doi:10.1016/j.enconman.2017.06.009.
29. *MATLAB 2019b*; © 1994-2020 The MathWorks, Inc.: Natick, Massachusetts, United States;
30. Eric W. Lemmon, Ian H. Bell, Marcia L. Huber, and Mark O. McLinden *REFPROP 10.0 Standard Reference Database 23*; National Institute of Standards and Technology, Boulder, Colorado, United States;
31. Product Catalogue | European Refrigerants Available online: https://www.honeywell-refrigerants.com/europe/product/tag/all-refrigerants/ (accessed on 18 June 2021).
32. "Fifth Assessment Report — IPCC." https://www.ipcc.ch/assessment-report/ar5/ (accessed Oct. 20, 2021).

33. H. Bell, P. A. Domanski, M. O. McLinden, and G. T. Linteris, “The hunt for nonflammable refrigerant blends to replace R-134a,” International Journal of Refrigeration, vol. 104, pp. 484–495, Aug. 2019, doi: 10.1016/j.ijrefrig.2019.05.035.
34. Accuvio Sustainability & Corporate Social Responsibility Data Software Solutions Annual Leakage Rate (%) for the Refrigeration/Air-Con/HVAC Available online: https://support.accuvio.com/support/solutions/articles/4000040366-annual-leakage-rate-for-the-refrigeration-air-con-hvac- (accessed on 7 May 2020).
35. Cerutti, A.K.; Duerr, M.; Iancu, A.; Janssens-Maenhout, G.; Koffi, B.; Kona, A.; Covenant of Mayors & Mayors Adapt Offices; European Commission; Joint Research Centre Covenant of Mayors for Climate and Energy: Default Emission Factors for Local Emission Inventories : Version 2017.; 2017; ISBN 978-92-79-71479-5.
36. Countries & Regions Energy Data - IEA Available online: https://www.iea.org/countries (accessed on 26 June 2020).